

# 4p states and X-Ray Spectroscopy

Jun-ichi Igarashi

*Faculty of Science, Ibaraki University, Mito, Ibaraki 310-8512, Japan*

Manabu Takahashi

*Faculty of Engineering, Gunma University, Kiryu, Gunma 376-8515, Japan*

The 4p states in transition metals and their compounds usually play minor roles on their physical quantities. Recent development of resonant x-ray scattering (RXS) at the *K*-edge of transition metals, however, casts light on the 4p states, because the signals on orbital and magnetic superlattice spots are brought about by the modulation in the 4p states. The 4p states are extending in solids and thereby sensitive to electronic states at neighboring sites. This characteristic determines the mechanism of RXS that the intensity on the orbital superlattice spots are mainly generated by the lattice distortion and those on magnetic superlattice spots by the coupling of the 4p states with the orbital polarization in the 3d states at neighboring sites. Taking up typical examples for orbital and magnetic RXS, we demonstrate these mechanisms on the basis of the band structure calculation. Finally, we study the MCD spectra at the *K*-edge, demonstrating that the same mechanism as the magnetic RXS is working.

## I. INTRODUCTION

X-ray scattering spectroscopy has attracted much attention after high brilliant synchrotron radiation became available. The scattering intensities are resonantly enhanced by tuning photon energy close to core excitations. This resonant x-ray scattering (RXS) is now widely used to investigate orbital and magnetic orders, since the resonant enhancement makes it possible to detect the weak intensities on superlattice Bragg spots.

In order to satisfy the Bragg condition on superlattice spots, the wave length of x-ray has to be an order of lattice spacing. This corresponds to *K*-edge energies, about 5 – 10 keV in transition metals. Actually the RXS at the *K*-edge has been carried out in transition-metal compounds for detecting signals on the orbital, magnetic, and charge superlattice spots.<sup>1,2,3,4,5,6,7,8,9,10,11,12,13,14,15,16,17,18,19,20,21,22,23</sup> The main peak of RXS may be described by a second-order process that a photon is virtually absorbed by exciting a core electron to unoccupied 4p states and then emitted by recombining the excited electron with the core hole. The problem is that the 4p states are not constituting the orbital order or the magnetic order, and this fact makes the interpretation of spectra unclear. How is the modulation brought about in the 4p states?

The 4p states of transition metals are well extended in solids and form a broad energy band with their widths > 20 eV. This fact indicates that simple tight-binding models are not suitable for the description of the 4p bands, but the band structure calculation is expected to work well. To obtain a feeling of the 4p state, we show in Fig. 1 the 4p wavefunction of a  $\text{Mn}^{3+}$  atom within the Hartree-Fock approximation, in comparison with the 3d wavefunction. As seen from the figure, 4p electrons have large probability in the interstitial region, indicating that they are sensitive to electronic structure at neighboring sites. This observation leads to important consequences

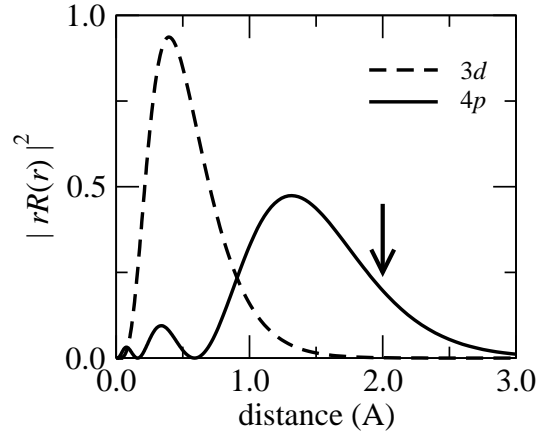


FIG. 1: 4p wave function of an atomic  $\text{Mn}^{3+}$  ion with a 1s core hole within the Hartree-Fock approximation. The arrow indicates the distance between the Mn nucleus and O nucleus in  $\text{LaMnO}_3$ .

on the mechanism of RXS; the intensity on orbital superlattice spots are mainly generated by the lattice distortion changing neighboring atom positions, and those on magnetic superlattice spots by the coupling of the 4p states with the orbital polarization (OP)<sup>69</sup> in the 3d states at neighboring site.

Taking up typical examples for orbital and magnetic RXS, we demonstrate that those mechanisms are actually working, on the basis of band structure calculations. Finally we discuss the mechanism of magnetic circular dichroism (MCD), which proves nearly the same as that of the magnetic RXS.

The present paper is organized as follows. In Sec. II, we study the RXS for both the orbital and magnetic orderings. In Sec. III, we discuss the MCD at the *K*-edge. Section IV is devoted to the concluding remarks.

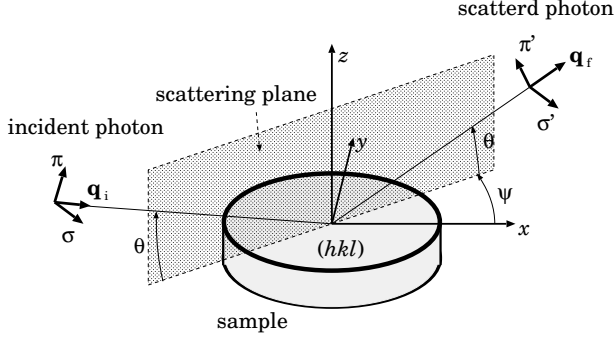


FIG. 2: Geometry of x-ray scattering. Incident photon with wave vector  $\mathbf{q}_i$  and polarization  $\sigma$  or  $\pi$  is scattered into the state with wave vector  $\mathbf{q}_f$  and polarization  $\sigma'$  or  $\pi'$  at Bragg angle  $\theta$ . The sample crystal is rotated by azimuthal angle  $\Psi$  around scattering vector  $\mathbf{G} = \mathbf{q}_f - \mathbf{q}_i$ .

## II. RESONANT X RAY SCATTERING

We start by a brief summary of the formulas of the RXS intensity. The scattering tensor can be approximated by a sum of contributions from each site where a core hole is created, since the  $1s$  state is well localized at transition-metal sites. Then the cross section for the scattering geometry shown in Fig. 2 is given by

$$\left. \frac{d\sigma}{d\Omega} \right|_{\mu \rightarrow \mu'} \propto \left| \sum_{\alpha\alpha'} P_{\alpha}^{\mu'} M_{\alpha\alpha'}(\mathbf{G}, \omega) P_{\alpha'}^{\mu} \right|^2, \quad (1)$$

with

$$M_{\alpha\alpha'}(\mathbf{G}, \omega) = \frac{1}{\sqrt{N}} \sum_j \exp(-i\mathbf{G} \cdot \mathbf{r}_j) \times \sum_{\Lambda} \frac{\langle \psi_g | x_{\alpha}(j) | \Lambda \rangle \langle \Lambda | x_{\alpha'}(j) | \psi_g \rangle}{\hbar\omega - (E_{\Lambda} - E_g) + i\Gamma}. \quad (2)$$

Here  $\mathbf{G} (= \mathbf{q}_f - \mathbf{q}_i)$  is the scattering vector, and  $\omega$  is the frequency of photon. Index  $j$  runs over transition-metal sites, the number of which is denoted as  $N$ . The cross section would become an order  $N$  on superlattice spots. The dipole operators  $x_{\alpha}(j)$ 's are defined as  $x_1(j) = x$ ,  $x_2(j) = y$ , and  $x_3(j) = z$  in the coordinate frame fixed to the crystal axes with the origin located at the center of site  $j$ . The ground-state energy and its wavefunction are defined as  $E_g$  and  $|\psi_g\rangle$ , respectively. State  $|\Lambda\rangle$  represents the intermediate state with energy  $E_{\Lambda}$ . Thus  $|\Lambda\rangle$  has the  $p$  symmetry with respect to the origin at the core-hole site. The  $\Gamma$  represents the life-time broadening width of the core hole, which is usually about 1 eV in transition-metal  $K$ -edges. The  $P^{\mu}$  and  $P^{\mu'}$  are the geometrical factors for incident and scattered photons with polarization  $\mu (= \sigma, \pi)$  and  $\mu' (= \sigma', \pi')$ , respectively.

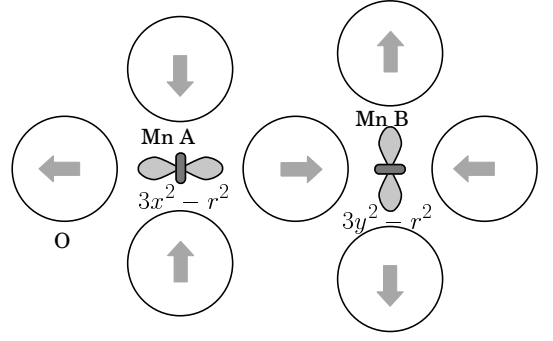


FIG. 3: Schematic view of the orbital order on the  $ab$  plane in  $\text{LaMnO}_3$ . Oxygen atoms move along the direction shown by arrows, which pattern is consistent with the orbital order.

### A. Orbital Order

The study of orbital order has attracted much interest since the discovery of colossal magnetoresistance in  $\text{La}_{1-x}\text{Sr}_x\text{MnO}_3$ <sup>24</sup>. The “orbital” is now recognized as an important factor for understanding the physics of transition-metal compounds. The neutron scattering has been very useful for the magnetic order, but is not so useful for the orbital order. Therefore a new method to probe the orbital order has been awaited. Then, Murakami et al. observed the RXS intensity at the  $K$ -edge on orbital superlattice spots, claiming that this signal is probing the orbital order<sup>9,10</sup>. But it was controversial how the spectra are related to the orbital order. We discuss this issue in the following.

#### 1. $e_g$ electron systems

We first consider  $\text{LaMnO}_3$ . In a localized picture of  $\text{Mn}^{3+}$  ion, three electrons occupy  $t_{2g}$  levels and one electron occupies  $e_g$  levels due to the Hund-rule coupling and the cubic crystal field. The double degeneracy of the  $e_g$  levels is lifted by the orbital-exchange coupling<sup>25</sup> or the cooperative Jahn-Teller effect.<sup>26</sup> Which is the driving force does not concern us in this paper. Irrespective to the driving force, the resulting orbital order and the crystal distortion are those shown in Fig. 3; the  $3x^2 - r^2$  and  $3y^2 - r^2$  orbitals are alternately arranged on the  $ab$  plane with oxygens positions shifted toward directions indicated by arrows.

As easily inferred from Eq. (2), the intermediate states ( $4p$  bands) have to be modulated in accordance with the orbital order for the RXS intensity not to vanish on the superlattice spots. If the anisotropic terms of the  $3d-4p$  Coulomb interaction is effective, the  $4p_x$  level becomes higher than the  $4p_y$  and  $4p_z$  levels for Mn sites with the  $3x^2 - r^2$  state, while the  $4p_y$  level becomes higher than the  $4p_x$  and  $4p_z$  levels for Mn sites with the  $3y^2 - r^2$  state. On the other hand, if the hybridization between the  $4p$  states and oxygen  $2p$  states at neighboring sites

is effective, the shifts of oxygen positions make the  $4p_y$  level higher than  $4p_x$  and  $4p_z$  levels for Mn sites with the  $3x^2 - r^2$  state while the  $4p_x$  level higher than  $4p_y$  and  $4p_z$  levels for Mn sites with  $3y^2 - r^2$  state. The two origins lead to the level shift opposite to each other. In solids, the  $4p$  states are not those localized levels but form energy bands with width of order 20 eV. Nevertheless, the tendency mentioned above on the  $4p$  levels would still hold in solids. At the early stage, Ishihara et al. interpreted the RXS signal on the orbital superlattice spots in  $\text{LaMnO}_3$  by the “Coulomb” mechanism.<sup>27,28</sup> By this mechanism, we could say that the modulation in  $4p$  bands is directly caused by the  $3d$  orbital order. However, subsequent studies based on band structure calculations have revealed that the Jahn-Teller distortion (JTD) gives rise to large RXS intensities.<sup>29,30,31</sup> We show in Fig. 4 the calculated spectra of the RXS intensity on an orbital superlattice spot in  $\text{LaMnO}_3$ .<sup>31</sup> The calculation is based on the local density approximation (LDA) within the muffin-tin (MT) approximation on the lattice parameters determined from the experiment. This approximate scheme leads to a small energy gap (0.2 eV) with a small orbital polarization. The “orbital” in this subsection means the levels with real wavefunctions such as  $3x^2 - r^2$ ,  $3y^2 - r^2$ ,  $p_x$ ,  $p_y$ ,  $p_z$ . In spite of this shortcoming for the  $3d$  bands, we expect that the  $4p$  bands are well described in the present calculation, since they have energies  $\sim 15$  eV higher than the  $3d$  bands and thereby the details of the  $3d$  bands are irrelevant. Actually, it was shown that the LDA+ $U$  method, which predicts a sufficient energy gap with large orbital polarization, gives the  $4p$  bands and the RXS spectra nearly the same as those given by the LDA method.<sup>32</sup> Since the MT approximation averages the potential coming from orbitally polarized  $3d$  states, it works to eliminate the effect of the anisotropic terms of the  $3d$ - $4p$  Coulomb interaction on the  $4p$  states. Thus, the calculated intensity is regarded purely generated by the JTD. The effect of the Coulomb interaction has been examined and estimated about two order of magnitude smaller than the JTD effect.<sup>31,32</sup> This finding is quite reasonable, since the  $4p$  states are well extended and sensitive to electronic states at neighboring sites.

Another typical example is  $\text{KCuF}_3$ . Each  $\text{Cu}^{2+}$  ion takes the  $3d^9$ -configuration, in which one hole occupies one of the  $e_g$  states. By the same reason as in  $\text{LaMnO}_3$ , the orbital order and the JTD take place. The band structure calculations<sup>33,34</sup> have been applied to evaluate the RXS intensity on the orbital superlattice spots in good agreement with the experiment,<sup>1</sup> clarifying that it arises mainly from the JTD.

As mentioned above, the  $4p$ -level shift by the JTD mechanism would be opposite to that by the Coulomb mechanism. Unfortunately, such difference in shift cannot be distinguished in antiferro-type orbital orders, due to a cancellation between different sublattices. The situation may be different in ferro-type orbital orders, but the actual detect of the difference is quite difficult be-

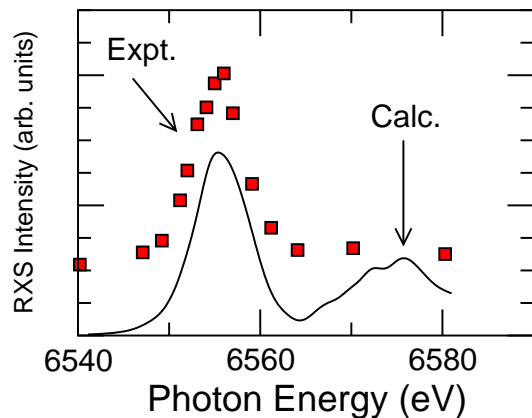


FIG. 4: Calculated RXS intensity on an superlattice spot at the  $K$ -edge in  $\text{LaMnO}_3$ , in comparison with the experiment.

cause of the overlapping fundamental-reflection intensities. To circumvent this difficulty, Kiyama et al.,<sup>35</sup> Ohsumi et al.<sup>17</sup> and Nakamura et al.<sup>11</sup> devised an interference technique and applied it to  $\text{La}_{0.45}\text{Sr}_{0.55}\text{MnO}_3$  and  $\text{La}_{0.60}\text{Sr}_{0.40}\text{MnO}_3$  multilayers. They have found that the level shift is indeed consistent with the JTD mechanism and opposite to the shift predicted by the Coulomb mechanism.

## 2. $t_{2g}$ electron systems

In  $t_{2g}$  electron systems such as  $\text{YTiO}_3$  and  $\text{YVO}_3$  where  $t_{2g}$  orbitals are partially occupied, the JTD is usually smaller than  $e_g$  electron systems such as  $\text{LaMnO}_3$  and  $\text{KCuF}_3$ . In such a situation, one may think the effect of Coulomb interaction important. This is not the case, though. Taking up the RXS in  $\text{YVO}_3$ , we demonstrate that the RXS spectra are mainly determined by the lattice distortion.<sup>36</sup>

This material takes three phases<sup>37</sup>: (a) a G-type antiferromagnetic state is developed with a moderate size of the JTD for  $T < 77$  K (the low-temperature (LT) phase); (b) a C-type antiferromagnetic state is developed with a small JTD for  $77 \text{ K} < T < 118$  K (the intermediate-temperature (IT) phase); (c) no magnetic order is developed but with a small JTD for  $118 \text{ K} < T$  (the high-temperature (HT) phase). In the three phases, the  $\text{GdFeO}_3$ -type distortion, the rotation and tilt of the  $\text{VO}_6$  octahedron, is intrinsically present in addition to the JTD, which makes the crystal belong to the space group  $Pbnm$ .

Noguchi et al.<sup>16</sup> have observed the RXS spectra at the  $K$ -edge of V, which are shown on the left panels in Fig. 5; three peaks are seen as a function of photon energy in the LT phase, while two peaks are suppressed with surviving one peak labeled “D<sub>2</sub>” in the IT phase. The RXS spectra are calculated based on the LDA and the MT approximation with the lattice parameters determined by the experiment. The result on the (100) reflection is shown

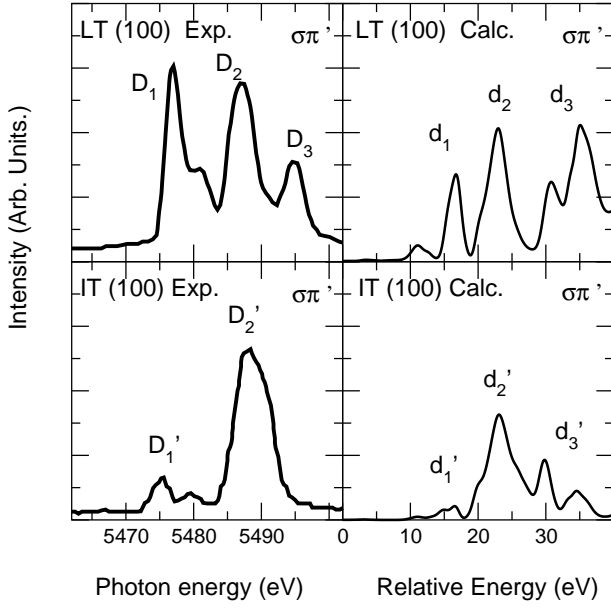


FIG. 5: RXS spectra on the (100) reflection at the  $K$ -edge in  $\text{YVO}_3$ . Right and left panels show the calculated spectra and the experimental data from Ref.16 ( $\Psi = 0$ ), respectively. Upper and lower panels are for the LT and IT phases, respectively.

on the right panels in Fig. 5.<sup>36</sup> Three peak structure is well reproduced. The spectra change drastically in the IT phase; peaks  $d_1$  and  $d_3$  are now strongly suppressed, although peak  $d_2$  keeps its strength. This behavior is in good agreement with the experiment. In addition, we have calculated the RXS spectra in an *imaginary* cubic crystal structure which has no  $\text{GdFeO}_3$ -type distortion but the JTD of the same type as in the real crystal, and have found that peak  $d_2$  is strongly suppressed but peaks  $d_1$  and  $d_3$  keep their strength.<sup>36</sup> This indicates that the contribution of the JTD is mainly concentrated to peaks  $D_1$  and  $D_3$  in the (100) reflection, while that of the  $\text{GdFeO}_3$ -type distortion is distributed to other peaks particularly peak  $D_2'$ . Calculating the RXS spectra with changing magnetic structures but with the same lattice distortion, we have confirmed that the magnetic structure affects little on the RXS spectra. This is consistent with the experimental finding that the RXS spectra in the HT phase are quite similar to those in the IT phase, because the main difference between the IT and HT phases are the presence or absence of magnetic order.

The experiment was first interpreted by the Coulomb mechanism.<sup>38</sup> This mechanism is unable to explain the three-peak structure and its difference between the LT and IT phases. The band calculation explains naturally most aspects of the spectra. Thereby we may conclude that the  $4p$  states are sensitive enough to the lattice distortion and that the RXS spectra are mainly controlled by the lattice distortion even in  $t_{2g}$  systems.

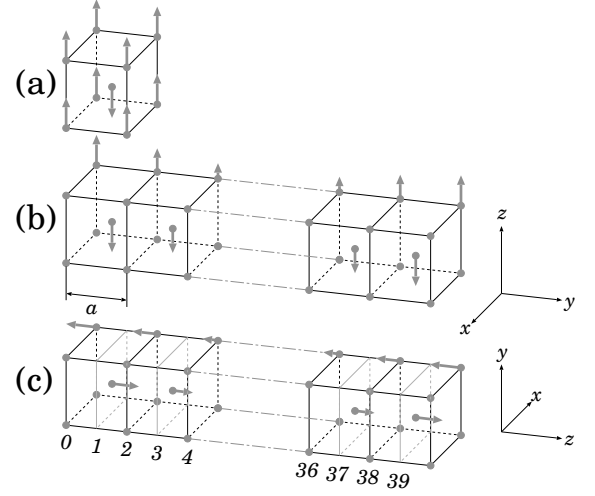


FIG. 6: Schematic view of the SDW state with  $Q_{\text{SDW}} = \frac{2\pi}{a} \frac{19}{20}$  with  $a$  the lattice constant of simple bcc structure. (a) A simple antiferromagnetic state. (b) A TSDW state. (c) An LSDW state. Integers indicate Cr site numbers.

## B. Magnetic Order

In magnetic materials, RXS signals are observed also on magnetic superlattice spots. The spin polarization alone could not give rise to the RXS intensity, because both the majority and minority spin states contribute to the scattering amplitude and thereby the scattering amplitudes are the same on all sites. The orbital polarization (OP) with respect to symmetries  $p_+ = \frac{1}{\sqrt{2}}(p_x + ip_y)$  and  $p_- = \frac{1}{\sqrt{2}}(p_x - ip_y)$  is necessary not to vanish the intensity. This is achieved by the spin-orbit interaction (SOI), which makes the orbital degrees of freedom couple to the spin polarization. The scattering amplitude  $M_{\alpha,\alpha'}$  has an antisymmetric form. Now a question is that how the spin order in the  $3d$  bands influence the OP in the  $4p$  bands. A natural answer lies again on the extended nature of the  $4p$  states. The OP is induced by the coupling to the OP in the  $3d$  bands at neighboring sites through the  $p$ - $d$  hybridization. We explain this scenario by taking up the spin density wave (SDW) phase in the Cr metal.<sup>39</sup>

The Cr metal forms a bcc lattice structure.<sup>40</sup> As cooling its magnetic state turns into a transverse spin density wave (TSDW) state at Néel temperature  $T_N = 311$  K and into a longitudinal spin density wave (LSDW) state at spin-flip temperature  $T_{\text{SF}} = 122$  K. In the TSDW (LSDW) state, magnetic moments are perpendicular (parallel) to the SDW propagation vector, as schematically shown in Fig. 6.

Although the wavelength of the SDW is incommensurate with the lattice periodicity, we approximate the SDW wavelength to be  $\lambda_{\text{SDW}} = 20a$  with  $a$  the bcc lattice constant. Thereby we are dealing with a large unit cell containing 40 inequivalent Cr atoms. This period is very close to the observed value at  $T_{\text{SF}}$ . We carry out

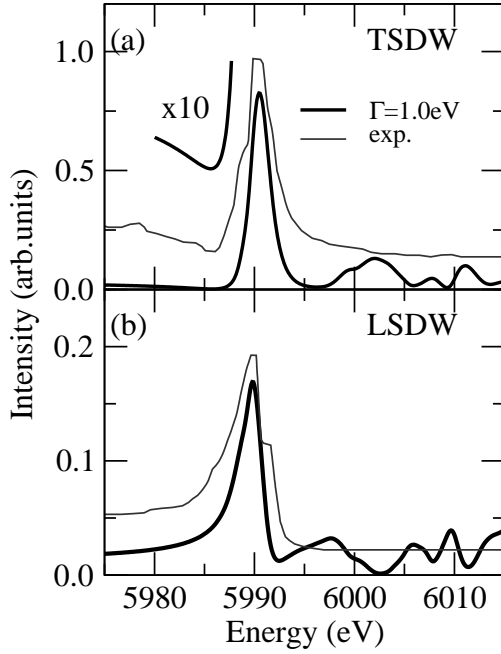


FIG. 7: (a) Calculated magnetic scattering intensities for  $\sigma\pi'$  channel on the SDW Bragg spot  $\mathbf{Q}_{\text{TSDW}}$  in the TSDW state. (b) Those on the spot  $\mathbf{Q}_{\text{LSDW}}$  in the LSDW state. The energy of the  $1s$  core level is assumed to be  $\epsilon_{1s} = \epsilon_F - 5988.4$  eV with  $\Gamma = 1.0$  eV. The experimental curve is traced from Ref.6.

the band calculation self-consistently with the large unit cell.<sup>39</sup> Within the LDA method and the MT approximation, we obtain the LSDW and TSDW phases as stable solutions with the magnetic moment written as

$$\mu_j = M_1 \cos(\mathbf{Q}_{\text{SDW}} \cdot \boldsymbol{\tau}_j) + M_3 \cos(3\mathbf{Q}_{\text{SDW}} \cdot \boldsymbol{\tau}_j) + M_5 \cos(5\mathbf{Q}_{\text{SDW}} \cdot \boldsymbol{\tau}_j) + \dots \quad (3)$$

Here  $\mathbf{Q}_{\text{SDW}}$  is a propagation vector of the SDW with  $\boldsymbol{\tau}_j$  denoting the position vector of the  $j$ th site ( $j = 0, 1, \dots, 39$  in Fig. 6). The magnetic moment is made up of the  $3d$  spin moment; the amplitudes in Eq. (??) are evaluated as  $M_1^{3d} = 0.393\hbar$ ,  $M_3^{3d} = -0.026\hbar$ ,  $M_5^{3d} = 0.0025\hbar$  in the LSDW state. These values are consistent with the reported band calculations<sup>41,42</sup> and the experiment.<sup>6</sup>

Then, adding the SOI term  $\frac{1}{r} \frac{d}{dr} V(r) \ell_z s_z$  to the MT potential  $V(r)$ , we calculate the eigenvalues and eigenfunctions, and finally calculate the magnetic RXS spectra. Figure 7 shows the calculated results in the LSDW and TSDW states,<sup>39</sup> in comparison with the experiment<sup>6</sup>. The calculation reproduces well not only the resonant behavior but also the Fano-type dip around  $\hbar\omega = 5986$  eV in the TSDW state. (The Fano phenomena arise from the interference between the resonant and non-resonant processes; we have omitted the description of the non-resonant term.)

How is the OP induced in the  $4p$  bands? This question is answered by calculating the RXS spectra with turning on and off the SOI on the  $p$  and  $d$  states selec-

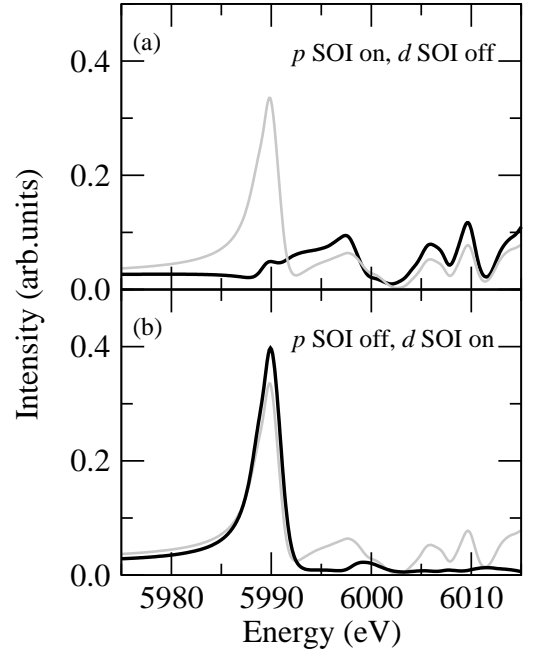


FIG. 8: Scattering intensity on the SDW spot  $\mathbf{Q}_{\text{LSDW}}$  in LSDW state. (a) The SOI in  $p$  state is turned on and the SOI in  $d$  state is turned off. (b) The SOI in  $p$  state is turned off and the SOI in  $d$  state is turned on. The gray lines represent the intensities calculated with both of the  $p$  SOI and  $d$  SOI being turned on.

tively. The result is shown in Fig. 8.<sup>39</sup> When the SOI is turned off only on the  $d$  states, the resonant main peak at  $\hbar\omega = 5990$  eV disappears, while the resonant structures at higher energies change little. On the other hand, when the SOI is turned off only on the  $p$  states, the main peak dose not change, while the resonant structure at higher energies almost disappears. Note that the  $p$  and  $d$  states do not hybridize each other at the same site because the SDW wavelength is so long that each site almost keeps the inversion symmetry. Therefore, the above finding indicates that the OP in the  $4p$  bands near the Fermi level, which gives rise to the main RXS peak, is mainly induced by the OP in the  $3d$  states at neighboring sites through the  $p$ - $d$  hybridization. Since the  $3d$  density of states is concentrated near the Fermi level, the  $p$ - $d$  hybridization may work effectively. It should be noted here that the orbital moment, which is given by the sum of the OP in the occupied levels, is found very small, but that the OP in the  $3d$  bands as a function of energy is found large (see Fig. 8 in Ref.39).

The fact that the OP in the  $4p$  bands is induced by the hybridization with the states at neighboring sites may be more clearly seen in the RXS for  $\text{UGa}_3$ , where a large peak at the  $K$ -edge of Ga is observed on the antiferromagnetic superlattice spots.<sup>7</sup> The OP in the  $4p$  states of Ga is induced through the hybridization with the  $5f$  states of U. Since the OP in the  $5f$  states of U is large, the induced OP in the  $4p$  states of Ga is also large, and

this gives rise to the large peak. The band structure calculation has confirmed this scenario<sup>43</sup>; when the SOI is turned off only on the 5f states, the peak is strongly suppressed.

In transition-metal compounds, the 4p bands are usually located more than 10 eV above the 3d bands. A typical example is NiO.<sup>3,15</sup> In such a situation, the effect of the hybridization with the 3d bands is not large. The band calculation has revealed that the OP in the 4p bands is mainly induced by the SOI on the 4p states.<sup>44</sup> This does not simply mean that the coupling to neighboring 3d states is unimportant, because the spin moment in the 4p bands is induced by the coupling to the spin moment in the 3d band. At any rate, the inducing mechanism is not simple here. As pointed out in the magnetic RXS, the same situation takes place in high energy states of the 4p bands in Cr metal.

### III. MAGNETIC CIRCULAR DICHROISM

We first summarize the formulas of MCD spectra. By neglecting the core-hole potential, the absorption coefficient for the right-handed (+) and left-handed (−) circular polarizations are calculated from

$$\mu_{\pm}(\omega) \propto \sum_{n,\mathbf{k}} \left| \int r^2 dr \int d\Omega \phi_{n,\mathbf{k}}(\mathbf{r})^* r Y_{1,\pm 1}(\Omega) R_{1s}(r) \right|^2 \times \theta(\epsilon_{n,\mathbf{k}} - \epsilon_F) \frac{\Gamma}{\pi (\hbar\omega - \epsilon_{n,\mathbf{k}})^2 + \Gamma^2}, \quad (4)$$

where the spherical harmonic function  $Y_{1,\pm 1}(\Omega)$  is defined with the quantization axis along the propagating direction of photon. The step function  $\theta(x)$  ensures that the sum is taken over states above the Fermi level. The  $R_{1s}$  represents the 1s wave function of transition metals, and  $\phi_{n,\mathbf{k}}$  represents the wave function with the band index  $n$ , wave-vector  $\mathbf{k}$  and energy  $\epsilon_{n,\mathbf{k}}$ . Equation (4) indicates clearly that only the  $p$  symmetric states contribute the intensity. Since the 4p states are extending, the assumption of neglecting the core-hole potential may be justified. The total absorption coefficient and the MCD spectra are defined by

$$\mu_0(\omega) = [\mu_+(\omega) + \mu_-(\omega)]/2 \quad (5)$$

$$\mu_c(\omega) = [\mu_+(\omega) - \mu_-(\omega)]. \quad (6)$$

As is clear from Eqs. (4) and (6), the MCD spectra at the  $K$ -edge probes the OP in the 4p bands, which situation is the same as the magnetic RXS at the  $K$ -edge. The main difference is that RXS could provide information on spatially modulated magnetic order such as antiferromagnetic states, while MCD is restricted on ferromagnetic states. In any case, the mechanism of inducing the OP in the 4p bands is closely related.

Ebert et al.<sup>45</sup> made an LDA calculation of the MCD spectra for Fe in good agreement with the experiment.<sup>46</sup>

A subsequent calculation for Ni,<sup>47</sup> however, gave merely semi-quantitative agreement with the experiment near the photothreshold. In addition, the underlying mechanism for the MCD was not clarified. One of the present author and Hirai<sup>48,49</sup> made a tight-binding calculation of the MCD spectra for Fe and Ni, where parameters were determined so as to fit the LDA band structure calculation. They not only reproduced well Ebert et al's result for Fe, but also obtained the spectra for Ni in good agreement with the experiment. They clarified the underlying mechanism by switching on and off the SOI selectively on the 4p and 3d states; the MCD spectra are mainly generated by the OP in the 3d states at neighboring sites through the  $p$ - $d$  hybridization. This mechanism has recently been reconfirmed by the calculation of the MCD spectra in Mn<sub>3</sub>GaC on the basis of the band calculation.<sup>50</sup> This example is discussed in detail in the following.

The Mn<sub>3</sub>GaC takes an “inverse” perovskite structure.<sup>51</sup> The magnetic property is that the antiferromagnetic phase in low temperatures turns into a ferromagnetic phase in high temperatures through a first-order transition at 168 K.<sup>52</sup> We carry out the band calculation assuming a ferromagnetic phase,<sup>50</sup> although an antiferromagnetic phase may be stabler than the ferromagnetic phase. The magnetization is obtained as  $\sim 0.8\mu_B$  per Mn. The SOI is introduced in the same way as in the calculation of the magnetic RXS spectra.

Figure 9 shows the calculated MCD spectra at the  $K$ -edge of Mn, in comparison with the experiment.<sup>52</sup> The calculated value of  $\mu_c(\omega)$  is divided by the value of  $\mu_0(\omega)$  at  $\hbar\omega = \epsilon_F + 20$  eV, while the experimental MCD spectra are divided by the value of the total absorption coefficient at the energy about 40 eV higher than the threshold. Both  $\mu_0(\omega)$  and  $\mu_c(\omega)$  are in good agreement with the experiment. For the total absorption coefficient, peaks A and B correspond well with shoulders A' and B' in the experimental curve. For the MCD spectra, dips C, D, and peak E correspond well with the experimental ones C', D', and E'. The underlying mechanism is clarified by calculating the MCD spectra at Mn sites with turning off the SOI on several specified states. The top panel among three panels of Fig. 9(c) shows the MCD spectra with turning off the SOI on all the states at Ga sites. The spectra remain similar except for a slight suppression of peak E, indicating that the OP at Ga sites have little influence on the MCD spectra at Mn sites. The middle panel of Fig. 9(c) shows the MCD spectra with turning off the SOI only on the  $p$  symmetric states at Mn sites. Dip C keeps the similar shape, while dip D almost vanishes. This indicates that the OP corresponding to dip D is induced by the spin polarization in the  $p$  symmetric states through the SOI in the 4p states. The bottom panel shows the MCD spectra with turning off the SOI only on the  $d$  symmetric states at Mn sites. The intensity of dip C is drastically reduced, but dip D and peak E remains similar, indicating that the OP in the 3d bands gives rise to dip C. Within the MT approximation,

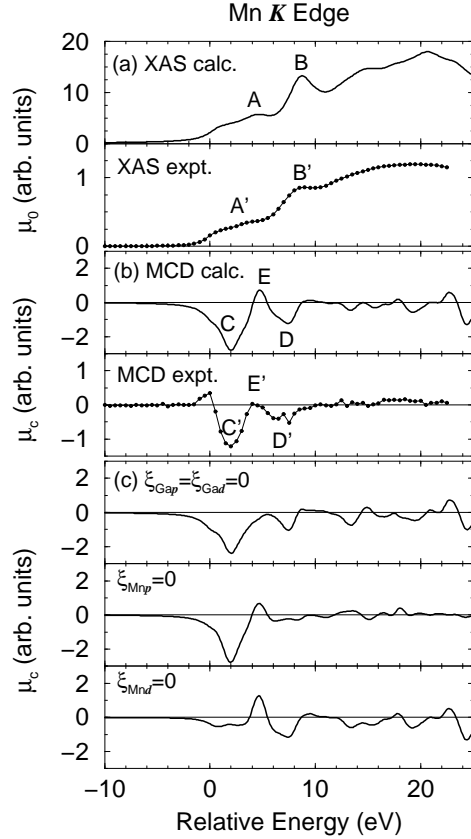


FIG. 9: Total absorption coefficient  $\mu_0(\omega)$  and MCD spectra  $\mu_c(\omega)$  at the  $K$ -edge of Mn, as a function of photon energy. The origin of energy corresponds to the excitation to the Fermi level. The experimental data are for a powdered sample in the ferromagnetic phase at  $T = 200$  K (Ref.50). (a)  $\mu_0(\omega)$ . (b)  $\mu_c(\omega)$ . (c)  $\mu_c(\omega)$  calculated with tuning off the SOI on all the states at Ga sites, on the  $p$  symmetric states at Mn sites, and on the  $d$  symmetric at Mn sites, respectively. ( $\xi_{Ab} = 0$  on panels indicates that the SOI on the  $b$  symmetric states at A sites is turned off.)

the  $3d$  OP cannot polarize the  $p$  orbital in the same Mn site, because the  $p$ - $d$  Coulomb interaction is spherically averaged inside the MT sphere. Thus we conclude that the OP corresponding to dip C is induced by the  $3d$  OP at *neighboring* Mn sites through the  $p$ - $d$  hybridization. Although the figure is not shown (see Fig. 3 in Ref.50), the MCD spectra are also observed at the  $K$ -edge of Ga. The same analysis has been applied to this case, clarifying that the OP in the  $4p$  states of Ga is mainly induced by the OP in the  $3d$  states of Mn at neighboring sites through the  $p$ - $d$  hybridization.

#### IV. CONCLUDING REMARKS

We have studied the mechanisms of RXS and MCD at the  $K$ -edge in transition metals and their compounds. The band structure calculations have proved powerful

enough to reproduce well the experimental spectra.

Analyzing in detail the cases for  $\text{LaMnO}_3$  and  $\text{YVO}_3$ , we have demonstrated that the RXS spectra on orbital superlattice spots arise mainly from the lattice distortion. Since the extended nature of the  $4p$  states naturally leads to sensitiveness to electronic structures at neighboring sites, this conclusion looks quite natural. The ‘‘Coulomb mechanism’’ is found irrelevant to the orbital RXS. In materials with extremely small lattice distortions, however, the anisotropic term of the intraatomic Coulomb interaction may play an important role. RXS spectra have been observed on quadrupole ordering spots at the Ce  $L_3$ -edge in  $\text{CeB}_6$ ,<sup>53</sup> in which any sizable lattice distortions have not been observed. A detailed analysis<sup>54,55</sup> has shown that the spectra are generated by modulating  $5d$  states through the intraatomic Coulomb interaction between the  $5d$  states and the orbitally polarized  $4f$  states.

In addition, analyzing the SDW phase of Cr, we have demonstrated that the RXS spectra on magnetic superlattice spots arise from the OP in the  $4p$  states, which is induced by the OP in the  $3d$  states at neighboring sites through the  $p$ - $d$  hybridization.

Finally we have discussed the mechanism of MCD spectra by taking the example of  $\text{Mn}_3\text{GaC}$ . We have emphasized a close relation to the mechanism of the MCD spectra at the  $K$ -edge. Again, it has been stressed that the  $4p$  states are extended and sensitive to electronic structures at neighboring sites.

We have not discussed the pre-edge peak at about 10 eV below the main peak. The intensity is usually one or two orders of magnitude smaller than the main-peak intensity. In the electric dipole transition, the relevant states must have the  $p$  symmetry with respect to the core-hole site. Since the energy of the peak corresponds to the excitation to the  $3d$  states, the  $p$  symmetric states have to be constructed by the  $3d$  states at neighboring sites. On the other hand, in the electric quadrupole transition, the relevant states have the  $d$  symmetry with respect to the core-hole sites. Therefore the  $d$  symmetric states are the  $3d$  states themselves. We could distinguish two processes by their azimuthal angle dependences of the spectra. The pre-edge peak observed on orbital superlattice spots in  $\text{YTiO}_3$  shows the same azimuthal angle dependence as the main peak, and thereby it is concluded to come from the dipole transition.<sup>4</sup> A possible pre-edge peak on the orbital superlattice spots in  $\text{LaMnO}_3$  has been analyzed in detail by the band calculation,<sup>56</sup> although the experimental confirmation has not been done yet. It is concluded that the dipole transition dominates the intensity. On the other hand, it is found that the pre-edge spectra on the magnetic superlattice spots in  $\text{NiO}$  arises from the quadrupole transition. The analysis based on the band calculation<sup>44</sup> has reproduced well the spectral pattern arising from the interference between the non-resonant process and the quadrupole process. Note that the distinction between  $p$  and  $d$  symmetries would lose the meaning in crystal structures without inversion symmetry, such as  $\text{V}_2\text{O}_3$  and  $\text{Cr}_2\text{O}_3$ .<sup>18,57,58,59,60,61</sup> An in-

interference between the dipole and quadrupole processes may become important.

If the RXS is available at the  $L_{2,3}$ -edge in transition metals, the spectra may be a direct probe to orbital and magnetic orders,<sup>62,63,64</sup> because the electric dipole transition excites an electron from the  $2p$  core to the  $3d$  states. The corresponding x-ray wave length is much larger than the lattice spacing, though. Recently, such attempts have been in progress to study orders with large periods and nanostructures.

Finally we comment the RXS at the  $M_{4,5}$ -edge in actinide compounds.<sup>65,66,67,68</sup> The dipole transition excites an electron from the  $3d$  core to the  $5f$  states, and the corresponding x-ray wavelength is an order of lattice spac-

ing. Therefore the RXS may become a direct probe to the  $5f$  states in order to study multipole orders such as quadrupole and octupole orders.

## Acknowledgments

We would like to thank N. Hamada, K. Hirai, T. Nagao, and M. Usuda for valuable discussions. This work was partially supported by a Grant-in-Aid for Scientific Research from the Ministry of Education, Culture, Sports, Science, and Technology, Japan.

- 
- <sup>1</sup> R. Caciuffo, L. Paolasini, A. Sollier, P. Ghigna, E. Pavarini, J. van den Brink, and M. Altarelli, Phys. Rev. B **65**, 174425 (2002).
  - <sup>2</sup> S. Di Matteo, T. Chatterji, Y. Joly, A. Stunault, J. A. Paixao, R. Suryanarayanan, G. Dhalenne, and A. Revcolevschi, Phys. Rev. B **68**, 024414 (2003).
  - <sup>3</sup> J. P. Hill, C.-C. Kao, and D. F. McMorrow, Phys. Rev. B **55**, R8662 (1997).
  - <sup>4</sup> M. Kubota, H. Nakao, Y. Murakami, Y. Taguchi, M. Iwama, and Y. Tokura, Phys. Rev. B **70**, 245125 (2004).
  - <sup>5</sup> J. E. Lorenzo, J. L. Hodeau, L. Paolasini, S. Lefloch, J. A. Alonso, and G. Demazeau, Phys. Rev. B **71**, 045128 (2005).
  - <sup>6</sup> D. Mannix, P. C. de Camargo, C. Giles, A. J. A. de Oliveira, F. Yokaichiya, and C. Vettier, Eur. Phys. J. B **20**, 19 (2001).
  - <sup>7</sup> D. Mannix, A. Stunault, N. Bernhoeft, L. Paolasini, G. H. Lander, C. Vettier, F. de Bergevin, D. Kaczorowski, and A. Czopnik, Phys. Rev. Lett. **86**, 4128 (2001).
  - <sup>8</sup> J. Herrero-Martín, J. Garcia, G. Subías, J. Blasco, and M. C. Sánchez, Phys. Rev. B **70**, 024408 (2004).
  - <sup>9</sup> Y. Murakami, J. P. Hill, D. Gibbs, M. Blume, I. Koyama, M. Tanaka, H. Kawata, T. Arima, Y. Tokura, K. Hirota, et al., Phys. Rev. Lett. **81**, 582 (1998).
  - <sup>10</sup> Y. Murakami, H. Kawata, M. Tanaka, T. Arima, Y. Moritomo, and Y. Tokura, Phys. Rev. Lett. **80**, 1932 (1998).
  - <sup>11</sup> M. Nakamura, M. Izumi, N. Ogawa, H. Ohsumi, Y. Wakabayashi, and K. Miyano, J. Phys. Soc. Jpn. **73**, 2802 (2004).
  - <sup>12</sup> H. Nakao, K. Ohwada, N. Takesue, Y. Fujii, M. Isobe, Y. Ueda, M. von Zimmermann, J. P. Hill, D. Gibbs, J. C. Woicik, et al., Phys. Rev. Lett. **85**, 4349 (2000).
  - <sup>13</sup> K. Namikawa, M. Ando, T. Nakajima, and H. Kawata, J. Phys. Soc. Jpn. **54**, 4099 (1985).
  - <sup>14</sup> W. Neubeck, C. Vettier, K.-B. Lee, and F. de Bergevin, Phys. Rev. B **60**, R9912 (1999).
  - <sup>15</sup> W. Neubeck, C. Vettier, F. de Bergevin, F. Yakhov, D. Mannix, O. Bengone, M. Alouani, and A. Barbier, Phys. Rev. B **63**, 134430 (2001).
  - <sup>16</sup> M. Noguchi, A. Nakazawa, T. Arima, Y. Wakabayashi, H. Nakao, and Y. Murakami, Phys. Rev. B **62**, R9271 (2000).
  - <sup>17</sup> H. Ohsumi, Y. Murakami, T. Kiyama, H. Nakao, M. Kubota, Y. Wakabayashi, Y. Konishi, M. Izumi, M. Kawasaki, and Y. Tokura, J. Phys. Soc. Jpn. **72**, 1006 (2003).
  - <sup>18</sup> L. Paolasini, C. Vettier, F. de Bergevin, F. Yakhov, D. Mannix, A. Stunault, W. Neubeck, M. Altarelli, M. Fabrizio, P. A. Metcalf, et al., Phys. Rev. Lett. **82**, 4719 (1999).
  - <sup>19</sup> L. Paolasini, R. Caciuffo, A. Sollier, P. Ghigna, and M. Altarelli, Phys. Rev. Lett. **88**, 106403 (2002).
  - <sup>20</sup> A. Stunault, F. de Bergevin, D. Wermeille, C. Vettier, T. Brückel, N. Bernhoeft, G. J. McIntyre, and J. Y. Henry, Phys. Rev. B **60**, 10170 (1999).
  - <sup>21</sup> G. Subías, J. Garcia, M. G. Proietti, J. Blasco, H. Renevier, J. L. Hodeau, and M. C. Sánchez, Phys. Rev. B **70**, 155105 (2004).
  - <sup>22</sup> M. von Zimmermann, J. P. Hill, D. Gibbs, M. Blume, D. Casa, B. Keimer, Y. Murakami, Y. Tomioka, and Y. Tokura, Phys. Rev. Lett. **83**, 4872 (1999).
  - <sup>23</sup> M. von Zimmermann, C. S. Nelson, Y.-J. Kim, J. P. Hill, D. Gibbs, H. Nakao, Y. Wakabayashi, Y. Murakami, Y. Tokura, Y. Tomioka, et al., Phys. Rev. B **64**, 064411 (2001).
  - <sup>24</sup> A. Urushibara, Y. Moritomo, T. Arima, A. Asamitsu, G. Kido, and Y. Tokura, Phys. Rev. B **51**, 14103 (1995).
  - <sup>25</sup> K. I. Kugel and D. I. Khomskii, JETP Lett. **15**, 446 (1972).
  - <sup>26</sup> J. Kanamori, J. Appl. Phys. Suppl. **31**, 14S (1960).
  - <sup>27</sup> S. Ishihara and S. Maekawa, Phys. Rev. Lett. **80**, 3799 (1998).
  - <sup>28</sup> S. Ishihara and S. Maekawa, Phys. Rev. B **58**, 13449 (1998).
  - <sup>29</sup> M. Benfatto, Y. Joly, and C. R. Natoli, Phys. Rev. Lett. **83**, 636 (1999).
  - <sup>30</sup> I. S. Elfimov, V. I. Anisimov, and G. A. Sawatzky, Phys. Rev. Lett. **82**, 4264 (1999).
  - <sup>31</sup> M. Takahashi, J. Igarashi, and P. Fulde, J. Phys. Soc. Jpn. **68**, 2530 (1999).
  - <sup>32</sup> P. Benedetti, J. van den Brink, E. Pavarini, A. Vigliante, and P. Wochner, Phys. Rev. B **63**, 060408 (2001).
  - <sup>33</sup> M. Takahashi, M. Usuda, and J. Igarashi, Phys. Rev. B **67**, 064425 (2003).
  - <sup>34</sup> N. Binggeli and M. Altarelli, Phys. Rev. B **70**, 085117 (2004).
  - <sup>35</sup> T. Kiyama, Y. Wakabayashi, H. Nakao, H. Ohsumi, Y. Murakami, M. Izumi, M. Kawasaki, and Y. Tokura, J. Phys. Soc. Jpn. **72**, 785 (2003).
  - <sup>36</sup> M. Takahashi and J. Igarashi, Phys. Rev. B **65**, 205114 (2002).



- (2002).
- <sup>37</sup> H. Kawano, H. Yoshizawa, and Y. Ueda, J. Phys. Soc. Jpn. **63**, 2857 (1994).
  - <sup>38</sup> S. Ishihara, T. Hatakeyama, and S. Maekawa, Phys. Rev. B **65**, 064442 (2002).
  - <sup>39</sup> M. Takahashi, J. Igarashi, and K. Hirai, Phys. Rev. B **70**, 174441 (2004).
  - <sup>40</sup> E. Fawcett, Rev. Mod. Phys. **60**, 209 (1988).
  - <sup>41</sup> K. Hirai, J. Phys. Soc. Jpn. **67**, 1776 (1998).
  - <sup>42</sup> R. Hafner, D. Spišák, R. Lorenz, and J. Hafner, Phys. Rev. B **65**, 184432 (2002).
  - <sup>43</sup> M. Usuda, J. Igarashi, and A. Kodama, Phys. Rev. B **69**, 224402 (2004).
  - <sup>44</sup> M. Usuda, M. Takahashi, and J. Igarashi, Phys. Rev. B **69**, 014408 (2004).
  - <sup>45</sup> H. Ebert, P. Strange, and B. L. Györfy, J. Appl. Phys. **63**, 3055 (1988).
  - <sup>46</sup> G. Schütz, W. Wagner, W. Wilhelm, P. Kienle, R. Zeller, R. Frahm, and G. Materlik, Phys. Rev. Lett. **58**, 737 (1987).
  - <sup>47</sup> S. Stähler, G. Schütz, and H. Ebert, Phys. Rev. B **47**, 818 (1993).
  - <sup>48</sup> J. Igarashi and K. Hirai, Phys. Rev. B **50**, 17820 (1994).
  - <sup>49</sup> J. Igarashi and K. Hirai, Phys. Rev. B **53**, 6442 (1996).
  - <sup>50</sup> M. Takahashi and J. Igarashi, Phys. Rev. B **67**, 245104 (2003).
  - <sup>51</sup> D. Fruchart and E. F. Bertaut, J. Phys. Soc. Jpn. **44**, 781 (1978).
  - <sup>52</sup> S. Uemoto, H. Maruyama, N. Kawamura, S. Umemura, N. Kitamoto, H. Nakao, S. Hara, M. Suzuki, D. Fruchart, and H. Yamazaki, J. Synchrotron Rad. **8**, 449 (2001).
  - <sup>53</sup> H. Nakao, K. Magishi, Y. Wakabayashi, Y. Murakami, K. Koyama, K. Hirota, Y. Endoh, and S. Kunii, J. Phys. Soc. Jpn. **70**, 1857 (2001).
  - <sup>54</sup> T. Nagao and J. Igarashi, J. Phys. Soc. Jpn. **70**, 2892 (2001).
  - <sup>55</sup> J. Igarashi and T. Nagao, J. Phys. Soc. Jpn. **71**, 1771 (2002).
  - <sup>56</sup> M. Takahashi, J. Igarashi, and P. Fulde, J. Phys. Soc. Jpn. **69**, 1614 (2000).
  - <sup>57</sup> M. Fabrizio, M. Altarelli, and M. Benfatto, Phys. Rev. Lett. **80**, 3400 (1998).
  - <sup>58</sup> A. Tanaka, J. Phys. Soc. Jpn. **71**, 1091 (2002).
  - <sup>59</sup> I. S. Elfimov, N. A. Skorikov, V. I. Anisimov, and G. A. Sawatzky, Phys. Rev. Lett. **88**, 015504 (2002).
  - <sup>60</sup> S. W. Lovesey, K. S. Knight, and D. S. Sivia, Phys. Rev. B **65**, 224402 (2002).
  - <sup>61</sup> Y. Joly, S. Di Matteo, and C. R. Natoli, Phys. Rev. B **69**, 224401 (2004).
  - <sup>62</sup> C. W. M. Castleton and M. Altarelli, Phys. Rev. B **62**, 1033 (2000).
  - <sup>63</sup> S. B. Wilkins, P. D. Hatton, M. D. Roper, D. Prabhakaran, and A. T. Boothroyd, Phys. Rev. Lett. **90**, 187201 (2003).
  - <sup>64</sup> S. B. Wilkins, P. D. Spencer, P. D. Hatton, S. P. Collins, M. D. Roper, D. Prabhakaran, and A. T. Boothroyd, Phys. Rev. Lett. **91**, 167205 (2003).
  - <sup>65</sup> E. D. Isaacs, D. B. McWhan, R. N. Kleiman, D. J. Bishop, G. E. Ice, P. Zschack, B. D. Gaulin, T. E. Mason, J. D. Garret, and W. J. L. Buyers, Phys. Rev. Lett. **65**, 3185 (1990).
  - <sup>66</sup> J. A. Paixão, C. Detlefs, M. J. Longfield, R. Caciuffo, P. Santini, N. Bernhoeft, J. Rebizant, and G. H. Lander, Phys. Rev. Lett. **89**, 187202 (2002).
  - <sup>67</sup> S. W. Lovesey, E. Balcar, C. Detlefs, G. van der Laan, D. S. Sivia, and U. Staub, J. Phys.: Condens. Matter **15**, 4511 (2003).
  - <sup>68</sup> T. Nagao and J. Igarashi, J. Phys. Soc. Jpn. **74**, 765 (2005).
  - <sup>69</sup> The orbital polarization means the difference in the density of states with respect to magnetic quantum numbers of the orbital angular momentum, as a function of energy.